AIP | The Journal of Chemical Physics

New implementation of the configuration-based multi-reference second order perturbation theory

Yibo Lei, Yubin Wang, Huixian Han, Qi Song, Bingbing Suo, and Zhenyi Wen

Citation: The Journal of Chemical Physics **137**, 144102 (2012); doi: 10.1063/1.4757264
View online: http://dx.doi.org/10.1063/1.4757264
View Table of Contents: http://scitation.aip.org/content/aip/journal/jcp/137/14?ver=pdfcov
Published by the AIP Publishing

New implementation of the configuration-based multi-reference second order perturbation theory

Yibo Lei,[1] Yubin Wang,[2] Huixian Han,[3] Qi Song,[2] Bingbing Suo,[2] and Zhenyi Wen[1,2,a)]
[1]*Key Laboratory of Synthetic and Natural Functional Molecule Chemistry of Ministry of Education, The College of Chemistry and Materials Science, Shaanxi Key Laboratory of Physico-Inorganic Chemistry, Northwest University, Xi'an 710069, People's Republic of China*
[2]*Institute of Modern Physics, Northwest University, Xi'an 710069, People's Republic of China*
[3]*Department of Physics, Northwest University, Xi'an 710069, People's Republic of China*

(Received 18 July 2012; accepted 20 September 2012; published online 9 October 2012)

We present an improved version of the configuration-based multi-reference second-order perturbation approach (CB-MRPT2) according to the formulation of Lindgren on perturbation theory of a degenerate model space. This version involves a reclassification of the perturbation functions and new algorithms to calculate matrix elements in the perturber energy expressions utilizing the graphical unitary group approach and the hole-particle symmetry. The diagonalize-then-perturb (DP), including Rayleigh-Schrödinger and Brillouin-Wigner, and diagonalize-then-perturb-then-diagonalize (DPD) modes have been implemented. The new CB-MRPT2 method is applied to several typical and interesting systems: (1) the vertical excitation energies for several states of CO and N_2, (2) energy comparison and timing of the ground state of C_4H_6, (3) the quasi-degeneracy of states in LiF, (4) the intruder state problems of AgH, and (5) the relative energies of di-copper-oxygen-ammonia complex isomers. The results indicate that the computational accuracy and efficiency of the presented methods are competitive and intruder-free. It should be emphasized that the DPD method rectifies naturally the shortcomings of LiF potential energy curves constructed by the original second order complete active space perturbation theory (CASPT2), without having to recourse to the so-called state mixture. Unlike CASPT2, the new methods give the same energy ordering for the two di-copper-oxygen-ammonia isomers as the previous multi-reference configuration interaction with single and double excitations methods. The new CB-MRPT2 method is shown to be a useful tool to study small to medium-sized systems. © *2012 American Institute of Physics*. [http://dx.doi.org/10.1063/1.4757264]

I. INTRODUCTION

Perturbation theory (PT), in particular, the second order Møller-Plesset (MP2) method is a simple, easy-to-use post-Hartree-Fock method.[1] It is well known that it works well for electronic states represented by a single non-degenerate Slater determinant, but often fails for states dominated by multi-configuration wave functions, degenerate or near degenerate.

To deal with general electronic states a variety of perturbation theory, the various versions of the multi-reference perturbation theory (MRPT), have been proposed during the last 30 years.[2–32] Currently, the most popular MRPTs are lower-order approaches, such as the multi-reference second order Møller-Plesset perturbation theory (MRMP2) and[8–10] second order complete active space perturbation theory (CASPT2).[7,11,21,25,27] Among them, the CASPT2 program developed by Roos and co-workers is very successful since it has dealt with a number of molecular systems and their electronic spectra. MRMP2 of Hirao *et al.* is similar to CASPT2. Both are state-specific and apply the same zeroth-order functions obtained by the complete active space self-consistent field (CASSCF) calculation, except that instead of using contracted configuration state function (CSF) as perturbation functions the former uses determinants. In addition, both adopt the diagonalize-then-perturb algorithm and cannot avoid the intruder states, although MRMP2 used a smaller shift in the denominator to remove the intruder states. Considering the possible degeneracy of different electronic states, CASPT2 and MRMP2 have developed respectively into multi-state (MS) CASPT2,[27,28] "extended" MS-CASPT2 (XMS-CASPT2),[34] multiconfiguration quasi-degenerate perturbation theory (MCQDPT),[13] and "extended" MCQDPT (XMCQDPT),[33] which are able to correct the errors of the original methods for the state with covalent–ionic avoided crossing of LiF at long distances and to improve the calculation accuracy.

Not long ago Chaudhuri *et al.*[35] evaluated some of the common multi-reference perturbation methods and proposed several characteristics for an ideal theoretical approach. The first is size extensivity and consistency. Unfortunately, currently widely used methods, such as CASPT2, do not have this characteristic.

According to the algorithm, perturbation approaches can be classified into two categories: orbital-based and configuration-based. The differences between the both mainly come from different definitions of the zeroth-order Hamiltonian H_0 and the method of computing the perturbation matrix elements. For the orbital-based method, H_0 is written as a sum of one-electron Fock operators containing orbital energies. This definition leads to the orbital energy

a)Electronic mail: wzy@nwu.edu.cn.

differences appearing in the denominator of the perturber energy expression. CASPT2 and MRMP2 belong to this category, which, generally speaking, are often accompanied by the intruder states, although there are many ways to remove them. For the configuration-based methods, H_0 is expressed as a sum of configuration projectors with energies, for example, the Epstein-Nesbet Hamiltonian. In this case it is the energy difference of two configurations instead of orbitals appearing in the denominator. However, since a configuration energy may be written as a sum of orbital energies and thence the configuration energy difference itself cannot prevent the intruder states, unless the single configuration energies are replaced by other energy terms. Shavitt's A_k method[6] is an example, in which one of the two single-configuration energies is replaced by the zeroth-order energy obtained by diagonalization of the model space. The N-electron valence state perturbation theory (NEVPT) method[36,37] provides another example. This method first divides the orbital space into three orbital subspaces of doubly occupied active and virtual orbitals and then defines eight function spaces $S_l^{(k)}$ consisting of perturbation functions, $\Psi_{l,\mu}^{(k)}$, generated by the orbital excitation operators acting on the reference functions. A $S_l^{(k)}$ space can further be split in two ways, resulting in two variants of NEVPT: strongly contraction subspace (one function $\Psi_l^{(k)}$ from each $S_l^{(k)}$) and partially contraction subspace $\bar{S}_l^{(k)}$composed of $\bar{\Psi}_{l,\mu}^{(k)}$, which are eigenfunctions of the model Hamiltonian in the subspace $\bar{S}_l^{(k)} \subset S_l^{(k)}$ with eigenvalues $\bar{E}_{l,\mu}^{(k)}$. Thus the energy denominator is $E_0 - E_l^{(k)}$ for strongly contraction or $E_0 - \bar{E}_{l,\mu}^{(k)}$ for partially contraction. Now NEVPT has been developed into quasi-degenerate (QD) NEVPT[37] which adopts the "diagonalize-then-perturb-then-diagonalize" (DPD) approach, where the second diagonalization is for H_{eff} matrix, whose basis is the corrected configuration functions by the first-order perturbation. QD-NEVPT is an interesting MRPT2 scheme and we will discuss it in Sec. III.

Recently, Mukherjee and co-workers[38] described a spin-adapted size-extensive state-specific multi-reference second-order perturbation theory (SA-SSMRPT2) based on the state-specific multi-reference coupled cluster (SSMRCC). As emphasized in the title, this approach is used to establish a size-extensive and state-specific theory. The former is of course encouraging, especially for the Brillouin-Wigner (BW) version, which is usually not considered to be size-extensive. The latter is limited to handle one state at a time for given space and spin symmetries.

In this work, we shall apply a perturbation treatment—the configuration-based multi-reference second order perturbation theory (CB-MRPT2), which is similar to QD-NEVPT but uses a different definition and classification of the perturbation functions, and completely different algorithms to calculate the matrix elements in the perturber energy expressions. In Sec. II, we will discuss the relevant theoretical background, particularly the graphical unitary group approach (GUGA) based on the hole-particle symmetry, which is the basis of implementing the new CB-MRPT2. A new specific algorithm is described in Sec. III, and then some applications are given in Sec. IV to show the capacity and efficiency of the new algorithm. Section V contains conclusive remarks.

II. THEORY

A. Graphical unitary group approach and hole-particle symmetry

GUGA is one of the most powerful methods for dealing with correlation energy calculations by using multi-reference configuration interaction with single and double excitations (MRCISD). Its main points can be summarized as follows:[39–48]

(a) The canonical basis of a unitary group $U(n)$, i.e. the set of functions symmetry-adapted to the subgroup chain,

$$U(n) \supset U(n-1) \supset \cdots \supset (2) \supset (1). \tag{1}$$

These functions are orthonormal and $\hat{S}^2$ conservative, hence is the best candidate of CSF.

(b) The canonical basis can be generated and stored in a graph—the Shavitt graph or distinct row table (DRT).

(c) For MRCISD, according to the electron occupation of orbitals of the reference states, a DRT can be divided into three parts: hole (doubly occupied), active, and external (virtual) orbital space.

(d) DRT in the external and hole space have very simple and similar structures (hole-particle symmetry) and thus is not constructed explicitly and only DRT in the active space needs to be generated explicitly.

(e) The DRT in the active space can be divided into many sub-DRTs, which are formed by taking one vertex located at the top and one at the bottom of the active space.

(f) The configuration interaction (CI) matrix elements can be determined by searching loops (coupling coefficients) in the DRT.

A schematic diagram for DRT is shown in Fig. 1. We note that in Fig. 1 the orbital space has been divided into three parts: n_h doubly occupied (hole), n_a active, and n_e virtual orbital spaces. Thus a complete step vector can be written as,[46]

$$|d\rangle \equiv |(d)_e(d)_c(d)_h\rangle. \tag{2}$$

where

$$(d)_e = (d_1 d_2 \cdots d_{n_e}),$$

$$(d)_c = (d_{n_e+1} d_{n_e+2} \cdots d_{n_e+n_a}),$$

$$(d)_h = (d_{n_e+n_a+1} d_{n_e+n_a+2} \cdots d_n).$$

For MRCISD, the allowed number of electrons excited is 0, 1, and 2. At the lower border of the active space there are four types of vertices: S, T, D, and V connecting to the external space, the number of paths from these vertices to the tail of the DRT, hereafter referred as number of down steps (NDF) are respectively equal to

$$\begin{aligned} NDF(V) &= 1, \\ NDF(D) &= n_e, \\ NDF(T) &= n_e(n_e-1)/2, \\ NDF(S) &= n_e(n_e+1)/2. \end{aligned} \tag{3}$$

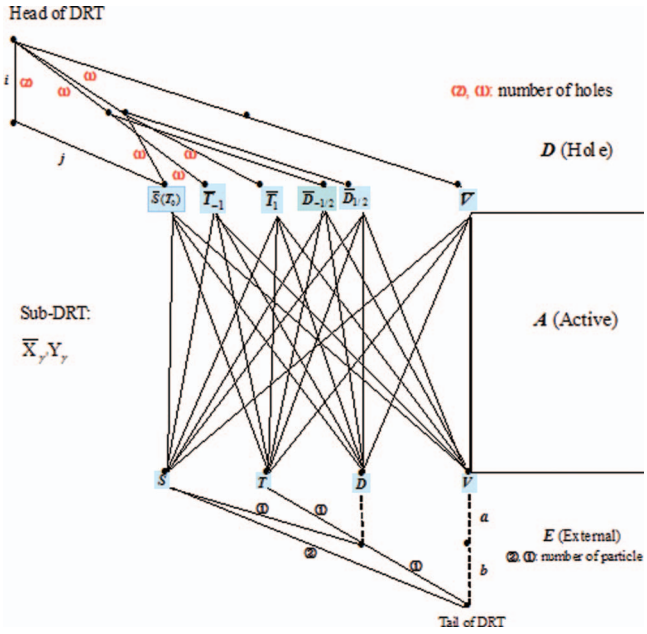

FIG. 1. Schematic diagram for DRT.

Similarly, at the upper border of the active space there may be six types of vertices: $\bar{S}$, $\bar{T}_{\pm 1}$, $\bar{D}_{\pm 1/2}$, and $\bar{V}$ connecting to the hole space. We can also similarly define the number of up steps (NUS). For $S = 0$, the formulas above are still correct but n_e must be replaced by n_h. However, for S > 0, the formula is slightly more complex.

In order to fully apply the hole-particle symmetry we shall divide the DRT in the active space into many sub-DRTs, which can be generated from a pair of vertices, each of the above and lower borders. Considering the symmetries of the vertices, the sub-DRT can be denoted as $\bar{X}_\gamma Y_{\gamma'}$, where γ and γ' are respectively the symmetry indices of the top and bottom vertices. In Fig. 1 we have marked the number of holes and particles connected to the sub-DRTs. If the dimension of a sub-DRT $\bar{X}_\gamma Y_{\gamma'}$ is Dim $(\bar{X}_\gamma Y_{\gamma'})$, then the total dimension of the full MRCISD can be written as

$$Dim(\text{MRCISD}) = \sum_{\bar{X}_\gamma Y_{\gamma'}} NUS(\vec{X}_\gamma) Dim(\vec{X}_\gamma Y_{\gamma'}) NDS(Y_{\gamma'}). \tag{4}$$

The matrix elements between CSFs can be expressed as

$$\langle (d)'|H|(d)\rangle = \sum_{p,q} \langle p|h_1|q\rangle C^{d'd}_{pq} + 1/2 \sum_{pqrs} \langle pr|h_{12}|qs\rangle C^{d'd}_{pq,rs}, \tag{5}$$

where $\langle p|h_1|q\rangle$ and $\langle pr|h_{12}|qs\rangle$ are one- and two-electron integrals, and

$$C^{d'd}_{pq} = \langle (d')|E_{pq}|(d)\rangle \tag{6}$$

$$C^{d'd}_{pq,rs} = \langle (d')|(E_{pq}E_{rs} - \delta_{qr}E_{pr})|(d)\rangle \tag{7}$$

are one- and two-electron coupling coefficients. Their calculations are the key to improving efficiency of matrix element computations. We consider calculations of the two-electron coupling coefficients,

$$\begin{aligned} C^{d'd}_{pq,rs} &= \langle (d')_h (d')_a (d')_e |(E_{pq}E_{rs} - \delta_{qr}E_{pr})|(d)_e (d)_a (d)_h\rangle \\ &= ELS \cdot ALS \cdot HLS. \end{aligned} \tag{8}$$

Here the factor of the active space has the form

$$ALS = W_0(pq, rs) + \omega W_1(pq, rs), \tag{9}$$

$$W_j(pq, rs) = \prod_{x=n_e+1}^{n_e+n_a} W(Q_x, d'_x d_x, \Delta b_x, b_x, j). \tag{10}$$

In Eq. (10), $W(Q_x; d'_x d_x, \Delta b_x, b_x, j)$ is called segment factor, in which Q_x is the segment factor type. The j appears only in the overlap area of the two generators and ω is a phase factor. *ELS, ALS*, and *HLS* are known as the external, active, and hole loop shape, respectively. Owing to the simple structure of DRTs in the external and the hole space, all possible values of *ELS* and *HLS* have been computed and written in the code of XI'AN-CI.[44,49] Therefore we only need to search loops and partial loops in the active space. In program XI'AN-CI, this approach has proven to be very effective.

B. Perturbation theory

For the CB-MRPT2, the complete configuration space is the MRCISD space that consists of reference configurations and single and double excitation configurations. As mentioned above, the configuration functions constitute a complete set of CSFs, which are orthonormal and S^2-symmetry adapted,

$$\langle \Phi_\mu | \Phi_\nu \rangle = \delta_{\mu\nu}, \mu, \nu = 1, 2, \cdots, Dim(\text{MRCISD}). \tag{11}$$

In perturbation methods the Hamiltonian H may be partitioned into a zeroth-order term H_0 and a perturbation V,

$$H = H_0 + V. \tag{12}$$

The zeroth-order Hamiltonian is defined as

$$H_0 = \sum_{\mu \in \text{MRCISD}} |\Phi_\mu\rangle E_\mu \langle \Phi_\mu|. \tag{13}$$

Obviously, from Eqs. (11) and (13), Φ_μ is an eigenfunction of H_0 with the eigenvalue E_μ,

$$H_0 \Phi_\mu = E_\mu \Phi_\mu. \tag{14}$$

Modern perturbation theory applies the so-called partitioning technique.[50] Its first step is to split the complete CSF set into two parts, a model space P and an orthogonal complement space Q and

$$P + Q = 1. \tag{15}$$

The projectors onto the P and Q spaces are, respectively,

$$P = \sum_{\alpha \in P} |\Phi_\alpha\rangle\langle\Phi_\alpha| \tag{16}$$

and

$$\mathrm{Q} = \sum_{\beta \in Q} |\Phi_\beta\rangle\langle\Phi_\beta|. \tag{17}$$

Thus the wave functions have been partitioned into two sets: $P\Psi$, which spans the model space, and $Q\Psi$, which spans the perturbation function space. The latter, in general, comes from single and double excitations of the reference configurations. The partition above means that a perturbation is equivalent to an excitation from the P space to the Q space and the zeroth-order Hamiltonian can be rewritten as

$$H_0 = \sum_{\alpha\in P} |\Phi_\alpha\rangle E_\alpha \langle\Phi_\alpha| + \sum_{\beta\in Q} |\Phi_\beta\rangle E_\beta \langle\Phi_\beta|. \tag{18}$$

By using the projectors P and Q on the Schrödinger equation, we obtain

$$\begin{pmatrix} PHP & PHQ \\ QHP & QHQ \end{pmatrix} \begin{pmatrix} P\Psi \\ Q\Psi \end{pmatrix} = E \begin{pmatrix} P\Psi \\ Q\Psi \end{pmatrix}. \tag{19}$$

As an approximation, the P space block PHP is first diagonalized, resulting in the zeroth-order function and energy Ψ_0 and E_0, while the Q space block QHQ only contains diagonal elements.[6] The perturbation theory will provide a procedure for gradually improving the wave function and energy starting from the zeroth-order wave function and energy. In this respect, the partitioning technique is to find effective operators that, when acting on the model space, can generate the same results as the original operators acting on the entire CSF space. For example, we can define an effective Hamiltonian H_{eff} that can, acting on the zeroth-order function, give the exact energy

$$H_{eff}\Psi_0 = E\Psi_0 \quad \text{or} \quad E = \langle\Psi_0|H_{eff}|\Psi_0\rangle. \tag{20}$$

Similarly, we can find an operator, called wave operator Ω, that will generate the exact wave function when acting on $\Psi_0 \in P$,

$$\Psi = \Omega\Psi_0. \tag{21}$$

Ψ and E are the exact function and exact energy, respectively. The two effective operators can be written in expanded forms,

$$\Omega = 1 + \Omega^{(1)} + \Omega^{(2)} + \cdots, \tag{22}$$

$$H_{eff} = H_0 + H_{eff}^{(1)} + H_{eff}^{(2)} + \cdots. \tag{23}$$

Their explicit form can be obtained by successive perturbation from the lower order terms to the higher order ones, and finally obtaining accurate wave functions and energies. For MRPT2 the expansions of Ω and H_{eff} consist of only the second and third terms, respectively. By using the partitioning technique it is straightforward to derive the perturber wave functions and the corresponding energies up to second order. However, we do not intend to give a detailed derivation because similar derivations can be found in many literatures.[51,52] Here we only list the formulae we need. For the Rayleigh-Schrödinger (RS) perturbation theory, the few lowest-order wave functions have the following forms:

$$\Psi_{R-S}^{(0)} = \Psi_0, \tag{24}$$

$$\Psi_{R-S}^{(1)} = \Omega^{(1)}\Psi_0 = \sum_{\beta\in Q} |\Phi_\beta\rangle \frac{\langle\Phi_\beta|V|\Psi_0\rangle}{E_0 - E_\beta}, \tag{25}$$

and the corresponding energies,

$$E^{(0)} = \langle\Psi_0|H_0|\Psi_0\rangle = \sum_{\alpha\in P} c_\alpha^2 E_\alpha, \tag{26}$$

$$E^{(1)} = \langle\Psi_0|H_{eff}^{(1)}|\Psi_0\rangle = \langle\Psi_0|V|\Psi_0\rangle, \tag{27}$$

$$E_{R-S}^{(2)} = \langle\Psi_0|H_{eff}^{(2)}|\Psi_0\rangle = \sum_{\beta\in Q} \frac{|\langle\Psi_0|V|\Phi_\beta\rangle|^2}{E_0 - E_\beta}. \tag{28}$$

In Eq. (28), E_0 is the sum of the zeroth- and first-order energies. If E_0 in the denominator are replaced by an unknown exact energy E, we obtain the zeroth- to second-order energies of the Brillouin-Wigner perturbation scheme,

$$E_{B-W}^{(0-2)} = E_0 + \sum_{\beta\in Q} \frac{|\langle\Psi_0|V|\Phi_\beta\rangle|^2}{E - E_\beta}. \tag{29}$$

Obviously, to obtain perturber energies from the Brillouin-Wigner energy expressions, a self-consistent iterative procedure is required.

III. ALGORITHM

A. Diagonalize then perturb approach

In the following discussion we assume that the model space is identical to the reference state space and only consider the MRPT2. Taking into account of the excited state calculations, we need several energy eigenvalues and eigenfunctions that are obtained by the diagonalization of the model space,

$$E_0^i, \Phi_0^i = \sum_{\alpha\in \mathrm{P}} c_\alpha^i \Phi_\alpha, \quad i = 1, 2, \cdots. \tag{30}$$

Thus the energy of the ith state up to second-order perturbation may be written in the form

$$\begin{aligned} E_{R-S}^i &= E_0^i + \sum_{\beta\in Q} \frac{\left|\langle\Phi_0^i|V|\Phi_\beta\rangle\right|^2}{E_0^i - E_\beta} \\ &= E_0^i + \sum_{\alpha\in P}\sum_{\beta\in Q} \frac{\left|\langle c_\alpha^i\Phi_\alpha|V|\Phi_\beta\rangle\right|^2}{E_0^i - E_\beta} \end{aligned} \tag{31}$$

for the Rayleigh-Schrödinger (RS) theory and

$$\begin{aligned} E_{B-W}^i &= E_0^i + \sum_{\beta\in Q} \frac{\left|\langle\Phi_0^i|V|\Phi_\beta\rangle\right|^2}{E - E_\beta} \\ &= E_0^i + \sum_{\alpha\in P}\sum_{\beta\in Q} \frac{\left|\langle c_\alpha^i\Phi_\alpha|V|\Phi_\beta\rangle\right|^2}{E - E_\beta}. \end{aligned} \tag{32}$$

for the Brillouin-Wigner theory.

According to our convention the reference space corresponds to the sub-DRT $\bar{V}V$, where the symmetry subscript has been omitted since V only allow a full-symmetric index. Applying the symbol introduced above, a reference CSF can be written as[46]

$$\begin{aligned} \Phi_R &= |(d)_e(d)_a(d)_h\rangle \\ &= |(00\cdots0)(d_{n_e+1}d_{n_e+2}\cdots d_{n_e+n_a})(33\cdots3)\rangle, \end{aligned} \tag{33}$$

TABLE I. (a) Classification of sub-DRTs.

(a) Classification of sub-DRTs

	Number of particles		
Number of holes	0	1	2
0	$\bar{V}V$	$\bar{V}D$	$\bar{V}S(T)$
1	$\bar{D}V$	$\bar{D}D$	$\bar{D}S(T)$
2	$\bar{S}(\bar{T})V$	$\bar{S}(\bar{T})D$	$\bar{S}(\bar{T})S(T)$

(b) Correspondence between $S_l^{(k)}$ and sub-DRTs

k[a]	0	0	1	−1	1	−1	2	−2
$S_l^{(k)}$	$S_{i,a}^{(0)}$	$S_{ij,ab}^{(0)}$	$S_i^{(1)}$	$S_a^{(-1)}$	$S_{ij,a}^{(1)}$	$S_{i,ab}^{(-1)}$	$S_{ij}^{(2)}$	$S_{ab}^{(-2)}$
Sub-DRTs	$\bar{D}D$	$\bar{P}P$	$\bar{D}V$	$\bar{D}P$	$\bar{P}D$	$\bar{D}P$	$\bar{P}V$	$\bar{V}P$

[a]k = No. of holes − no. of particles. $P = S$ or T, $\bar{P} = \bar{S}$ or $\bar{T}$.

which is easy to check from Fig. 1. The perturbation functions Φ_β are involved in the sub-DRTs $\bar{X}Y$ except $\bar{V}V$. Hereafter the set of functions belonging to a sub-DRT $\bar{X}Y$ is denoted as $\Phi(\bar{X}Y)$. For instance $\Phi(\bar{V}V)$ represents the reference CSFs. It can be seen from Eq. (31) and (32) that the perturber energy depends on the computation of the matrix elements between excited and reference CSFs. But before that, we compare $\bar{X}Y$ with the space $S_l^{(k)}$,[36,37] to which the perturbation functions $\Psi_{l,\mu}^{(k)}$ in second order NEVPT (NEVPT2) belong. Table I illustrates the number of holes and particles in connection with $\bar{X}Y$ and their correspondence with the eight classes of spaces $S_l^{(k)}$. The correspondence is obvious if the index k is defined as the difference of the number of holes and particles. However, the correspondence between the perturbation functions $\Phi(\bar{X}Y)$ and $\Psi_l^{(k)}$ is not clear. It seems from the definition in Eq. (6) of Ref. 37 that $\Psi_l^{(k)}$ is a set of contracted functions but $\Phi(\bar{X}Y)$ is uncontracted. Moreover, the algorithm utilized in this work will be different from that used in NEVPT2.

Now we consider calculations of the matrix elements, and first of all, the coupling coefficients,

$$\begin{aligned} C_{pq}^{\beta\alpha} &= \langle\Phi_\beta|E_{pq}|\Phi_\alpha\rangle, \\ C_{pq,rs}^{\beta\alpha} &= \langle\Phi_\beta|(E_{pq}E_{rs} - \delta_{qr}E_{ps})|\Phi_\alpha\rangle, \\ \alpha \in P &\equiv \bar{V}V, \beta \in Q = \bar{X}_\gamma Y_{\gamma'}, \end{aligned} \tag{34}$$

In GUGA, we shall search loops and partial loops between $\bar{X}_\gamma Y_{\gamma'}(X, Y \neq V)$ and $\bar{V}V$. As shown in Eq. (33), the reference CSFs have very simple hole and external steps: all the hole steps are equal to 3, and all the external steps are 0, which lead to only five possible combinations of segment factors,

(a) A_R–A^R,
(b) D_{RR}–D^{RR},
(c) D_{RR}–B^R–A^R,
(d) A_R–B_R–D^{RR},
(e) A_R–B_R–B^R–A^R.

Table II compiles all possible partial loops, as well as the hole and external loop shapes connecting to the partial loops between $\bar{X}Y$ and $\bar{V}V$. The resulting coupling coefficients and matrix elements are used in Eqs. (31) and (32) to obtain the RS and BW energy up to second-order perturbation. This algorithm is proven to be very effective.

B. An extended model space

In order to accelerate the convergence of the perturbation series and avoid the intruder state, we can choose a larger model space. The new model space includes all the internally excited configurations, i.e.,

$$P = \bar{V}V + \bar{D}V + \bar{T}V + \bar{S}V. \tag{35}$$

Apparently, the larger model space will reduce the perturbative contribution but will increase the calculation cost since for model space larger than the reference space there are more possible combinations of segment factors in calculations of the coupling coefficients. The efficiency should be lower than the smaller model space although the hole-particle symmetry still provides an effective algorithm.

C. Diagonalize-then-perturb-then-diagonalize approach

The single-state CASPT2 cannot correctly describe potential energy curves at the avoided crossing region of LiF molecule, the MRPT2 based on the diagonalize- then-perturb approach also does not work. For CASPT2, this problem can be solved by the improved variants of MS-CASPT2 and XMS-CASPT2 through redefining the Fock operator,[28,34] which is obviously inconvenient for CB-MRPT2 approach. We notice that when we apply MRPT2 approach, either RS-MRPT2 (Eq. (31)) or BW-MRPT2 (Eq. (32)), the energy is second-order, while the wave function is not truly first-order due to the presence of the unchanged zeroth-order configuration coefficients in the second-order energy term. This conflict may result in anomalous behavior of the potential energy curves in near degeneracy situations, such as the violation of the non-crossing rule for the two-atom potential energy curves. As an evidence, the CASSCF function as the zeroth-order perturbation approximation gives at least correct behavior of the curves. The diagonalize-then-perturb-then-diagonalize[37,53] may be a better approach, in which we are not concerned with the single-electron basis (although, it may be useful for improving accuracy) but define a correct first-order perturbation function. Once the true first-order perturbation functions are obtained, reasonable configuration functions and effective Hamiltonian matrix H_{eff} up to second-order can be formed and its diagonalization produces the reasonable

TABLE II. Calculations of coupling coefficients.[a]

	HLS[b]	*ALS*	*ELS*[c]
$\bar{V}D$		A_R-	$W_0 = W_1 = -1$
		$A_R-B_R-B^R-$	
$\bar{V}T$		A_R-B_R-	$W_0 = 0, W_1 = -1$
$\bar{V}S$		A_R-B_R-	$W_0 = 0, W_1 = -\sqrt{1/2}$
			$W_0 = 0, W_1 = -\sqrt{2}$
		$D_{RR}-$	$W_0 = 0, W_1 = -1$
			$W_0 = 0, W_1 = -\sqrt{2}$
$\bar{D}D$		$-B_R-B^R-$	$W_0 = W_1 = -1$
$\bar{D}T$	$W_0 = W_1 = -(-1)^{2S}\sqrt{(2S+2)/(2S+1)}$	$-B_R-$	$W_0 = 0, W_1 = -1$
$\bar{D}S$		$-B_R-$	$W_0 = -1, W_1 = 0$
			$W_0 = W_1 = -\sqrt{2}$
$\bar{T}D$		$-B^R-$	$W_0 = W_1 = -1$
$\bar{T}T$	$W_0 = 0, W_1 = -(-1)^{2S}\sqrt{(2S+3)/(2S+1)}$	$-C''-$	$W_0 = 0, W_1 = -1$
$\bar{T}S$	$W_0 = 0, W_1 = (-1)^{2S}\sqrt{(2S-1)/(2S+1)}$	$-C''-$	$W_0 = -1, W_1 = 0$
			$W_0 = W_1 = -\sqrt{2}$
$\bar{S}D$	$W_0 = \sqrt{\frac{2S}{4S+2}}, W_1 = \sqrt{\frac{2S+2}{4S+2}}$	$-B^R-$	$W_0 = W_1 = -1$
$\bar{S}T$	$W_0 = \sqrt{\frac{2S+2}{4S+2}}, W_1 = -\sqrt{\frac{2S}{4S+2}}$	$-C''-$	$W_0 = 0, W_1 = -1$
$\bar{S}S$	$W_0 = -\sqrt{2}, W_1 = 0$	$-C''-$	$W_0 = -1, W_1 = 0$
			$W_0 = W_1 = -\sqrt{2}$

[a] $\langle (d)_e (d)_a (d)_h | [E_{pq} + \frac{1}{2} e_{pq,rs}] | (d)_h (d)_a (d)_e \rangle = HLS \times ALS \times ELS$.
[b] Possible hole loop shapes $\bar{D}$: A_R-; $\bar{T}$: $A_R - B_R-$; $\bar{S}$: $D_{RR}-$, $A_R - B_R -$.
[c] Possible external loop shapes D: $-A^R$; T: $- B^R - A^R$; S: $- D^{RR}$; $- B^R - A^R$.

second-order system energy. Let us write the CI wave function defined in the model space in the form,

$$\Phi = \sum_{\alpha \in P} \tilde{C}_\alpha \tilde{\Phi}_\alpha, \tag{36}$$

where

$$|\tilde{\Phi}_\alpha\rangle = |\Phi_\alpha\rangle + \sum_{\beta \in Q} |\Phi_\beta\rangle \frac{H_{\beta\alpha}}{E_0 - E_\beta}, \tag{37}$$

$$H_{\beta\alpha} = \langle \Phi_\beta | H | \Phi_\alpha \rangle = \langle \Phi_\beta | V | \Phi_\alpha \rangle. \tag{38}$$

The configuration functions are orthonormal up to the second order perturber energy, i.e.,

$$\langle \tilde{\Phi}_\alpha | \tilde{\Phi}_{\alpha'} \rangle = \delta_{\alpha\alpha'} + 0(\lambda^2). \tag{39}$$

The eigenvalue equation to be solved is

$$H_{eff}^{(0-2)} \Phi = E \Phi, \tag{40}$$

and the CI matrix elements can be written as

$$\left(H_{eff}^{(0-2)}\right)_{\alpha\alpha'} = \langle \Phi_\alpha | H | \Phi_{\alpha'} \rangle + \sum_{\beta \in Q} \frac{\langle \Phi_\alpha | V | \Phi_\beta \rangle \langle \Phi_\beta | V | \Phi_{\alpha'} \rangle}{E_0 - E_\beta}. \tag{41}$$

We will see in the following test calculations that the wrong behaviors of the potential curves produced by diagonalization of the $H_{eff}^{(0-2)}$ matrix no longer exist, which is expected for a normal MRCISD calculation. However, the energy E_0 arising in the denominator of Eq. (41) still contains the zeroth-order configuration coefficients which may affect the accuracy of computed energies. Actually, it can be seen from the derivation process of the RS perturbative expansion that the zeroth-order energy E_0 can be replaced by other energies. For example, If E_0 is substituted by E_0' generated by the $H_{eff}^{(0-2)}$ diagonalization and the diagonalization is carried out again, we may obtain an improved total energy. This procedure differs from the BW-MRPT2 calculation. The latter is to improve energy iteratively until convergence while the former is to improve the wave operator and there is no convergence requirement.

IV. APPLICATIONS

In this section, we present some applications of the new CB-MRPT2 to demonstrate its capability and efficiency. In the following calculations we used GAMESS-US[54] or MOLCAS7.5[55] quantum chemistry packages for the CASSCF calculations, which provide the molecular orbital integrals required for matrix element calculations.

A. Vertical excitation energies for several states of CO and N_2

Table III lists the vertical excitation energies for seven states of CO and eight states of N_2. Besides the present work we choose results from two different MRPT2 methods, CASPT2 taken from MOLPRO[56,57] and intruder state avoid (ISA)-MRMP with level shift parameter of 0.08 a.u. directly from literature.[58] The same basis set aug-cc-pVTZ[59,60] and reference space CAS (10,8) are chosen for both systems. It can be seen that the BW-MRPT2 with the larger model space (LBW-MRPT2) results in the smallest average deviation from experiments:[61] 0.05 and 0.16 eV for N_2 and CO, respectively. The superior performance of LBW-MRPT2 is evident in this example. The larger RS-MRPT2 (LRS-MRPT2) results are also displayed in this table. It should be noticed that although

TABLE III. Vertical excitation energy comparisons for CO and N_2 (eV).[a]

Molecule	State	CASPT2[b]	ISA-MRMP[c]	MRPT2 (BW)	MRPT2[d] (LBW)	Exp.[e]
CO	$^1\Sigma^-$	9.88	9.90	9.92	9.91	9.88
	$^1\Pi$	8.34	8.40	8.41	8.41	8.51
	$^1\Delta$	9.80	9.99	10.14	10.15	10.23
	$^3\Sigma^+$	8.18	8.24	8.32	8.31	8.54
	$^3\Sigma^-$	9.51	9.64	9.62	9.62	9.88
	$^3\Pi$	6.08	6.02	6.10	6.10	6.32
	$^3\Delta$	9.02	9.16	9.13	9.13	9.36
	Error	**0.27**	**0.20**	**0.16**	**0.16**	
N_2	$^1\Sigma_u^-$	9.65	9.96	9.92	9.92	9.92
	$^1\Pi_g$	9.09	9.25	9.74	9.42	9.31
	$^1\Delta_u$	10.01	10.28	10.33	10.32	10.27
	$^3\Sigma_u^+$	7.45	7.50	7.92	7.92	7.75
	$^3\Sigma_u^-$	9.40	9.56	9.68	9.68	9.67
	$^3\Pi_g$	7.82	7.87	8.08	8.07	8.04
	$^3\Pi_u$	10.92	10.95	11.83	11.24	11.19
	$^3\Delta_u$	8.63	8.82	8.89	8.89	8.88
	Error	**0.26**	**0.12**	**0.17**	**0.05**	

[a]Basis set: aug-cc-pVTZ, active space: CAS(10,8), equilibrium bond length: 2.08 a.u. for N_2 and 2.14 a.u. for CO.
[b]CASPT2 with 0.3 a.u. level shift (Refs. 56 and 57).
[c]Ref. 58.
[d]Equilibrium bond length for CO is 2.07 a.u.
[e]Ref. 61.

the energy gaps for CO calculated by BW-MRPT2 is almost equal to those by LBW-MRPT2 the average deviation for N_2 evaluated by the former method is larger than those by the latter. These results strengthen the conclusion that the larger model space may be conducive to improve the computational accuracy.

B. The comparison of computation efficiency for the ground state of C_4H_6

In Table IV, we present timings for several methods on the ground state computations of trans-butadiene C_4H_6. The molecular geometry is given in the supplementary material.[62] The basis set and reference space are respectively cc-pVDZ[59] and CAS (6,7), where $3b_u$, (1-3)b_g, and (1-3)a_u are the active orbitals and (1-2)a_g and (1-2)b_u are frozen. It can be seen from the data presented in Table IV that the CASPT2 program in MOLCAS7.5[55] is the fastest, while the similar program in MOLPRO[56,57] is much slower. The BW-MRPT2 calculation in the large model space (LBW-MRPT2) is obviously slowest, but is closest to MRCISD in energy.

We note that DPD-MRPT2 method is also very effective and can produce quite accurate energies. The high efficiency is the superiority of GUGA based on the hole-particle symmetry and the accurate energy originates from an additional iteration when the iterative convergence is almost completed. Moreover, the present algorithm may be improved if the contraction approximation is utilized. As can be seen from Table IV, the dimension of the contracted CI space is only 1/24 of the uncontracted space. Hence utilization of the contracted functions should be able to improve the computation efficiency.

TABLE IV. The comparison of several methods on the computation of ground state of C_4H_6 with the reference space of CAS(6,7).[a]

Method	P space[b]	CI DIM	Energies (a.u.)	Run time(s)[c]
RS-MRPT2[d]	149		−155.5418552	3.52
BW-MRPT2[d]	149		−155.4582586	32.14
DPD-MRPT2[d]	149		−155.4501397	8.06
LRS-MRPT2[d]	10 827		−155.5377969	6.84
LBW-MRPT2[d]	10 827		−155.4572225	69.98
CASPT2[e]	149		−155.4805737	31.82
CASPT2[f]	149		−155.4779754	0.79
MCQDPT2[g]	149		−155.4843290	14.56
IC-MRCI[e]		977 805	−155.4593803	841.13
MRCI[d]		24 255 498	−155.4627182	3821.28

[a]Basis set: cc-PVDZ, uncorrelated orbital: 4.
[b]Reference space of different MRPT approaches.
[c]Calculations are performed on a single core of an Xeon processor (2.27 GHz).
[d]Present methods are included in our program package Xian-CI (Ref. 49).
[e]MOLPRO2010.1 (Refs. 56 and 57).
[f]MOLCAS7.5 (Ref. 55).
[g]GAMESS-US (Ref. 54).

C. The quasi-degeneracy of LiF potential energy curves

As the potential energy curves of LiF are one of standard benchmark test for the quasi-degenerate perturbation theory,[13,28,33,34,63] we evaluate the $^1\Sigma^+$ potential energy curves of LiF for its ground and first excited state in the region of the ionic-neutral avoided crossing by using the BW-MRPT2 and DPD-MRPT2 variants of the present MRPT2 and CASPT2 in MOLCAS7.5.[55] The aug-cc-pVTZ[59,60] basis sets for both Li and F atoms are adopted and CAS (6,6) is taken as the reference space, which are the same as the very recent test[34] for both XMS-CASPT2 and MRCISD. The perturbation functions are not contracted in the present calculation. The results are displayed in Fig. 2.

The BW-MRPT2 curves cross twice at about 10.71 a.u. and 14.08 a.u., violating the non-crossing rule. Similar situation appears in the orbital-based single-state-CASPT2 (SS-CASPT2)[11] computation. We note that the $^1\Sigma^+$ potential

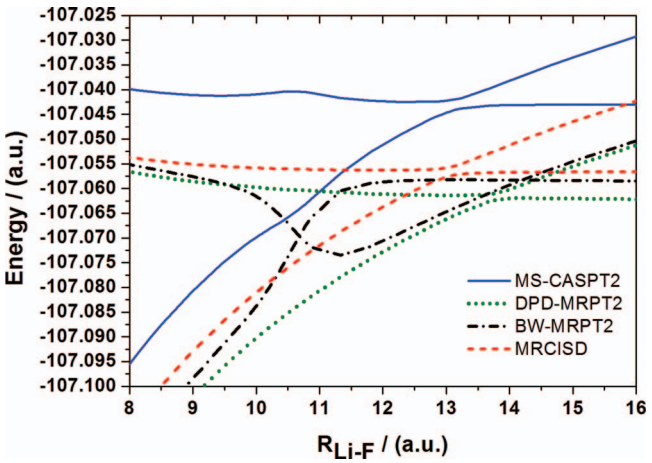

FIG. 2. LiF potential energy curves computed by CASPT2, MRCISD, BW-MRPT2, and DPD-MRPT2. Blue solid curves: MS-CASPT2; green dotted curves: DPD-MRPT2; black dashed–dotted curves: BW-MRPT2; and red dashed curves: MRCISD.

curves of LiF obtained by DPD-MRPT2 and MS-CASPT2 calculations demonstrate only one avoided crossing around 13.76 a.u. and 13.21 a.u. respectively, in good qualitative agreement with the more accurate MRCISD calculations with avoid crossing at 13.00 a.u. It can be clearly seen from Fig. 2 that the DPD-MRPT2 curves are closer to those of MRCISD and more smooth than MS-CASPT2,[28] but the location of the avoided crossing is slightly farther away from that of MR-CISD than MS-CASPT2.

D. Potential energy curves of AgH

As reported previously, MRMP calculations result in many singularities on the potential energy curves (PECs) of AgH.[58] For example, there are eight for $2^1\Delta$ and 11 for $3^1\Delta$ state. All the singularities can be removed by introducing energy shifts in the denominator of the second-order perturber energy expression. In this work, the MS-CASPT2 by MOLCAS7.5[28,55] and the present DPD-MRPT2 calculations are performed to test whether these singularities still exist. For the singlet we select the basis set atomic natural orbital type with triple-zeta plus polarization quality (ANO-RCC-VTZP)[64] and active space CAS (12,10), where the 10 active orbitals are $5a_1$, $2b_1$, $2b_2$, and $1a_2$, and the reference space contains 3392 CSFs. A state average CASSCF of four states are performed employing MOLCAS7.5 program[55] to provide molecular integrals for the following CASPT2 and DPD-MRPT2 calculations.

The curves for the two singlets of $2^1\Delta$ and $3^1\Delta$ mapped by MS-CASPT2 with 0.0 and 0.3 a.u. energy shift and DPD-MRPT2 are plotted in Figures 3(a)–3(c), respectively. It can be found from Figure 3(a) that four singularity points are found at around 4.12 a.u. of interatomic distance of AgH in the two curves, and the singularity points disappear in Figure 3(b), thanks to the introduction of the 0.3 a.u. level shift. In Figure 3(c) we see two smooth curves, which suggest that the present MPRT2 approaches are intruder-free because of the large energy difference in the denominator of Eqs. (31) and (32).

E. Relative energies of di-copper-oxygen-ammonia complex isomers

As the final example, we calculated the energies of two representative isomers of di-copper-oxygen complexes with six ammonia ligands $\{[Cu(NH_3)_3]_2O_2\}^{2+}$. The two isomers are bis-oxo and peroxo forms, labeled as **iso-1** and **iso-2** thereafter. With regard to the relative stability of the two isomers, the previous theoretical studies demonstrated obvious disagreements.[65–68] The more stable isomer evaluated by the CASPT2 approach is **iso-1**, in disagreement with **iso-2** computed by density functional theory (DFT) and other theoretical levels, as the former overestimates energy of **iso-1** relative to **iso-2** by 20-30 kcal mol^{-1}.[65] This molecule is a challenge for CASPT2 approaches and a typical system for testing the accuracy of the present DPD-MRPT2 methods.

In this work, the geometries of these two isomers are taken from a recent article of Rode and Werner and the chosen

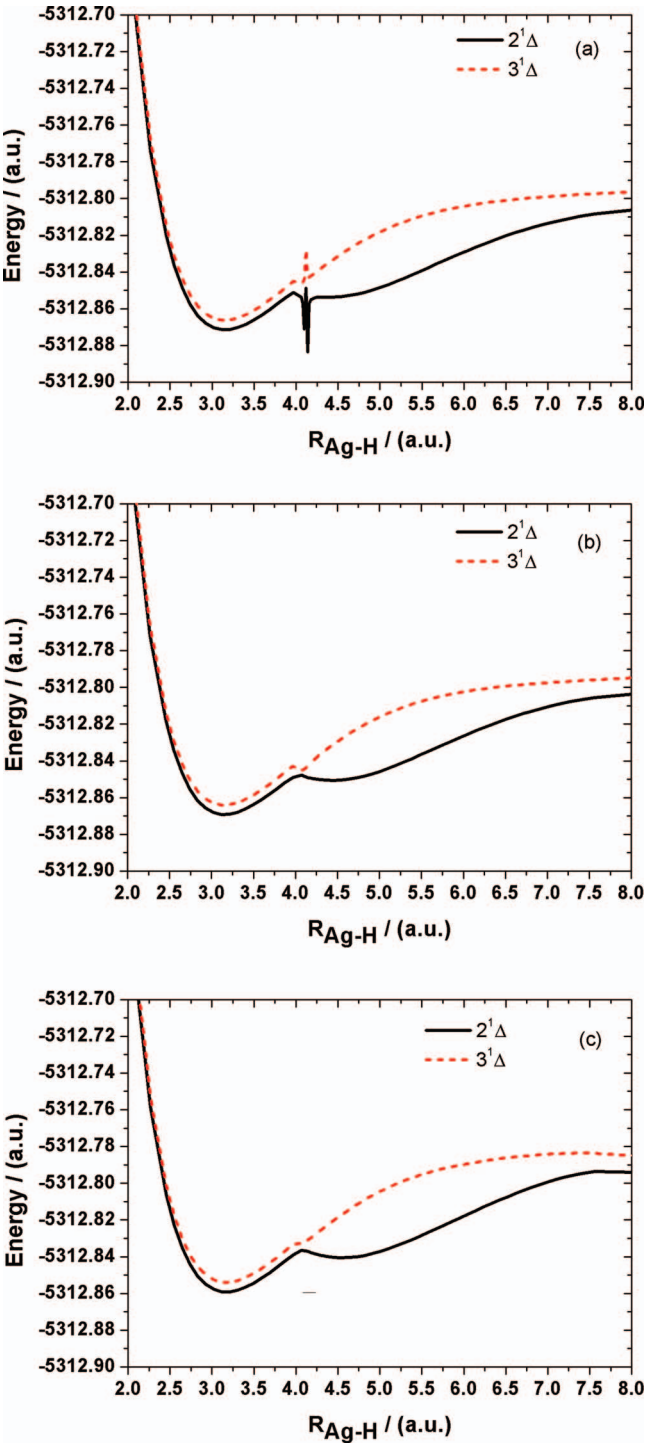

FIG. 3. Potential energy curves for the $2^1\Delta$ and $3^1\Delta$ of AgH calculated using (a) MS-CASPT2 without level shift; (b) MS-CASPT2 with 0.3 a.u. level shift; and (c) DPD-MRPT2.

active spaces CAS(8,6), CAS(8,10) are the same as used in their work.[66] We employed the Stuttgart pseudopotential and associated basis functions for Cu[69] including the relativistic effects, the aug-cc-pVDZ basis sets[60] for O and N, and DZP basis set for H.[70] Except for the basis set of Cu, the other basis sets were consistent with those in the work of Rode and Werner[66] so that it can also be denoted AVDZ. As reported recently,[66] even larger basis set cannot influence the energy order of these two isomers, so the chosen AVDZ here is at

TABLE V. Comparisons of Energy differences $\Delta E = E(\textbf{iso-1}) - E(\textbf{iso-2})$ (in kcal mol^{-1}) of di-copper complexes computed with different methods and active spaces.

Method	AVDZ[a]	AVTZ[a,b]	FP[c]	This work[d]
UKS/B3LYP	16.69	15.29	19.9	
RKS/B3LYP	6.14	4.08	14.4	
CASSCF(8,6)				25.80
CASPT2(8,6)	− 8.85	− 12.21		− 2.46
BW-MRPT2(8,6)				**15.31**
DPD-MRPT2(8,6)				**17.11**
MRCI(8,6)		16.0		
MRCI(8,6)+Q	12.42	11.1		
BW-MRPT2(8,8)				**8.84**
DPD-MRPT2(8,8)				**11.56**
CASSCF(8,10)	23.90	23.44	23.2	21.77
CASPT2(8,10)	− 7.37	− 10.24	− 11.5	− 2.14
BW-MRPT2(8,10)				**12.43**
DPD-MRPT2(8,10)				**13.83**
MRCI(8,10)		14.6		
MRCI(8,10)+Q		9.8		

[a]Reference 64.
[b]Reference 65.
[c]Reference 66.
[d]All CASSCF, CASPT2, BW, and DPD-MRPT2 calculations using the basis set AVDZ.

least qualitatively sufficient to evaluate the energies of **iso-1** relative to **iso-2**. Like the very recent MRCISD calculation,[66] 16 core orbitals were frozen for the following DPD-MRPT2 and CASPT2 calculations. The number of correlated orbitals (including double occupied and active orbitals) of CAS(8,6) is 42, breaking through the limitation of the maximum 32 in MOLPRO program.[56,57] The computational details were described in the supplementary material.[62]

The energy difference $\Delta E = E(\textbf{iso-1}) - E(\textbf{iso-2})$ of di-copper complexes computed in this work and some previous results are displayed in Table V. It can be seen that all CASPT2 calculations lead to negative energy differences. This stabilizes **iso-2** relative to **iso-1**. Since the current work just focuses on the comparison of the previous results with those of the new methods, detailed discussion of the CASPT2 results is ignored. Employing relatively small basis set and the active space of CAS(8,6), our DPD- and BW-MRPT2 results of 15.31 and 17.11 kcal mol^{-1} are both consistent with previously estimated value of 16.0 kcal mol^{-1} by MRCISD calculation. So is with CAS(8,10).[66] Based on these results, the present DPD-MRPT2 method might be able to predict energy differences of transition metal complexes.

V. CONCLUSIONS

In this work we described an improved version of the CB-MRPT2 based on the formulation of Lindgren with regard to the perturbation theory of a degenerate model space.[51] The older version has been applied to construct potential energy surfaces of several molecules[71–75] but the computation size and efficiency are limited from the algorithm. As we see in the text, in the new algorithm we suggest different formulas for different sets of perturbation functions. Both the diagonalize-then-perturb and diagonalize-then-perturb-then-diagonalize models have been implemented. The computer codes for the present methods have been included in the XIAN-CI program package.[44,49]

As applications of the present methods, some test calculations for several currently hot issues are performed. The results show that the present approaches are valuable for dealing with these problems. We specially emphasize the DPD-MRPT2 method, which can be considered to be an approximate MRCISD and consequently is capable to rectify naturally the shortcomings of the original CASPT2 potential energy curves without recourse to the so-called state mixture because in the CI method these "states" have been mixed. For the DPD-MRPT2 computation based on uncontracted CSFs, the $\{[Cu(NH_3)_3]O_2\}^{2+}$ complex is a rather difficult issue since with the basis set of aug-cc-PVDZ, reference CAS (8,10) and 42 correlation orbitals, the number of the CSFs reaches 116 161 742 872, which seems to be a configuration space that has never been dealt with up to now. For the DPD-MRPT2 calculation, of course, the real CI space is the model space that contains only 3540 configuration functions generated from the above CSFs. In order to improve the accuracy of perturbative calculations, even higher-order perturbation than MRCISD can be used but the costs will greatly increase. However, these calculations are possible if contractive functions are employed. For instance, the strong contraction schemes (one sub-DRT is contracted into one function except the reference space) will reduce the number of configurations mentioned above to 19 429 098, which is obviously a feasible CI space. With this contraction, the computation cost will be further reduced and this work is underway.

ACKNOWLEDGMENTS

The authors are grateful to Dr. Z. Zhang from Stanford University for useful discussions. This work is supported by the National Natural Science Foundation of China (NNSFC) (Project Nos.: 21003100, 21033001, 21103136, and 21173166).

[1]C. Møller and M. S. Plesset, Phys. Rev. **46**, 618 (1934).
[2]M. G. Sheppard and K. F. Freed, J. Chem. Phys. **75**, 4507 (1981).
[3]B. O. Ross, P. Linse, P. E. M. Siegbahn, and M. R. A. Blomberg, Chem. Phys. **66**, 197 (1982).
[4]K. Andersson, P. Å. Malmqvist, B. O. Roos, A. J. Sadlej, and K. Wolinski, J. Phys. Chem. **94**, 5483 (1990).
[5]D. Maynau and J.-L. Heully, Chem. Phys. Lett. **187**, 295 (1991).
[6]I. Shavitt, Chem. Phys. Lett. **192**, 135 (1992).
[7]K. Andersson, P. Å. Malmqvist, and B. O. Roos, J. Chem. Phys. **96**, 1218 (1992).
[8]K. Hirao, Chem. Phys. Lett. **190**, 374 (1992).
[9]K. Hirao, Chem. Phys. Lett. **196**, 397 (1992).
[10]K. Hirao, Chem. Phys. Lett. **201**, 59 (1993).
[11]K. Andersson and B. O. Roos, Int. J. Quantum Chem. **45**, 591 (1993).
[12]C. H. Martin, R. L. Graham, and K. F. Freed, J. Chem. Phys. **99**, 7833 (1993).
[13]H. Nakano, J. Chem. Phys. **99**, 7983 (1993).
[14]P. M. Kozlowski and E. R. Davidson, J. Chem. Phys. **100**, 3672 (1994).
[15]P. M. Kozlowski and E. R. Davidson, Chem. Phys. Lett. **222**, 615 (1994); **226**, 440 (1994).
[16]J. Stevens, R. L. Graham, and K. F. Freed, J. Chem. Phys. **101**, 4832 (1994).
[17]A. Zaitseveskii and J. P. Malrieu, Chem. Phys. Lett. **238**, 597 (1995); **250**, 366 (1996).
[18]J. P. Finley, Chem. Phys. Lett. **318**, 190 (2000); J. P. Finley and H. A. Witek, J. Chem. Phys. **112**, 3958 (2000); C. Angeli, R. Cimiraglia, S. Evangelisti,

T. Leininger, and J.-P. Malrieu, *ibid.* **114**, 10252 (2001); Y.-K. Choe, Y. Nakano, and K. Hirao, *ibid.* **115**, 621 (2001); C. Angeli, B. Bories, A. Cavallini, and R. Cimiraglia, *ibid.* **124**, 054108 (2006); M. Miyajima, Y. Watanabe, and H. Nakano, *ibid.* **124**, 044101 (2006); Chem. Phys. Lett. **442**, 164 (2007); A. Szabados, J. Chem. Phys. **134**, 174113 (2011); H. Nakano, R. Uchiyama, and K. Hirao, J. Comput. Chem. **23**, 1166 (2002); U. S. Mahapatra, S. Chattopadhyay, and R. K. Chaudhuri, J. Chem. Phys. **129**, 024108 (2008); **130**, 014101 (2009); J. Comput. Chem. **32**, 325 (2011).
[19]J. P. Finley and K. F. Freed, J. Chem. Phys. **102**, 1306 (1995).
[20]K. G. Dyall, J. Chem. Phys. **102**, 4909 (1995).
[21]B. O. Roos and K. Andersson, Chem. Phys. Lett. **245**, 215 (1995).
[22]H. J. Werner, Mol. Phys. **89**, 645 (1996).
[23]M. R. Hoffmann, J. Phys. Chem. **100**, 6125 (1996).
[24]R. Cimiraglia, Int. J. Quantum Chem. **60**, 167 (1996).
[25]B. O. Roos, K. Andersson, M. P. Fülscher, P.-Å. Malmqvist, L. Serrana-Andrés, L. Pierloot, and M. Merchán, in *Advances in Chemical Physics: New Methods in Computational Quantum Mechanics*, edited by I. Prigogine and S. A. Rice (Wiley, New York, 1996), Vol. XCIII, p. 219.
[26]H. Nakano, K. Nakayama, K. Hirao, and M. Dupuis, J. Chem. Phys. **106**, 4912 (1997).
[27]N. Fersberg and P. A. Maimqvist, Chem. Phys. Lett. **274**, 196 (1997).
[28]J. Finley, P.-Å. Malmqvist, B. O. Roos, and L. Serrano-Andrés, Chem. Phys. Lett. **288**, 299 (1998).
[29]W. Wenzel and M. M. Steiner, J. Chem. Phys. **108**, 4714 (1998).
[30]J. P. Finley, J. Chem. Phys. **108**, 1081 (1998).
[31]Y. Wang, Z. Gan, K. Su, and Z. Wen, Sci. China **B43**, 567 (1999).
[32]M. Forés and L. Adamowicz, J. Comput. Chem. **20**, 1422 (1999).
[33]A. A. Granovsky, J. Chem. Phys. **134**, 214113 (2011).
[34]T. Shiozaki, W. Győrffy, P. Celani, and H.-J. Werner, J. Chem. Phys. **135**, 081106 (2011).
[35]R. K. Chaudhuri, K. F. Freed, G. Hose, P. Piecuch, K. Kowalski, M. Włoch, S. Chattopadhyay, D. Mukherjee, Z. Rolik, Á. Szabados, G. Tóth, and P. R. Surján, J. Chem. Phys. **122**, 134105 (2005).
[36]C. Angeli, R. Cimiraglia, and J.-P. Malrieu, J. Chem. Phys. **117**, 9138 (2002).
[37]C. Angeli, S. Borini, M. Cestari, and R. Cimiraglia, J. Chem. Phys. **121**, 4043 (2004).
[38]S. Mao, L. Cheng, W. Liu, and D. Mukherjee, J. Chem. Phys. **136**, 024105 (2012); **136**, 024106 (2012).
[39]J. Paldus, J. Chem. Phys. **61**, 5321 (1974).
[40]J. Paldus, in *The Unitary Group Approach for the Evaluation of the Electronic Energy Matrix Elements*, edited by J. Hinze (Springer, Berlin, 1981), p. 1.
[41]I. Shavitt, in *The Unitary Group Approach for the Evaluation of the Electronic Energy Matrix Elements*, edited by J. Hinze (Springer, Berlin, 1981), p. 51.
[42]I. Shavitt, in *Mathematical Frontiers in Computational Chemical Physics*, edited by D. G. Truhlar (Springer-Verlag, New York, 1988), p. 299.
[43]P. W. Payne, Int. J. Quantum Chem. **22**, 1085 (1982).
[44]Y. Wang, Z. Wen, Q. Du, and Z. Zhang, J. Comput. Chem. **13**, 187 (1992).
[45]Z. Gan, Y. Wang, and Z. Wen, J. Comput. Chem. **22**, 560 (2001).
[46]Y. Wang, G. Zhai, B. Suo, Z. Gan, and Z. Wen, Chem. Phys. Lett. **375**, 134 (2003).
[47]Y. Wang, B. Suo, G. Zhai, and Z. Wen, Chem. Phys. Lett. **389**, 315 (2004).
[48]B. Suo, G. Zhai, Y. Wang, Z. Wen, X. Hu, and L. Li, J. Comput. Chem. **26**, 88 (2005); Y. Lei, B. Suo, Y. Dou, Y. Wang, and Z. Wen, *ibid.* **31**, 1752 (2010).
[49]Z. Wen, Y. Wang, Z. Gan, B. Suo, and Y. Lei, XI'AN-CI, a program package for electronic correlation energy calculations, see http://www.sccas.cn/gb/cooper/cooper15/index.html.
[50]P.-O. Löwdin, J. Math. Phys. **3**, 969 (1962); **3**, 1171 (1962).
[51]I. Lindgren and J. Morrison, *Atomic Many-Body Theory* (Springer-Verlag, Berlin Heidberg, 1982).
[52]S. Wilson, *Electron Correlation in Molecules* (Oxford University Press, London, 1984).
[53]H. Wang, Y. G. Khait, and M. R. Hoffmann, Mol. Phys. **103**, 263 (2005).
[54]M. W. Schmidt, K. K. Baldridge, J. A. Boatz, S. T. Elbert, M. S. Gordon, J. H. Jensen, S. Koseki, N. Matsunaga, K. A. Nguyen, S. J. Su, T. L. Windus, M. Dupuis, and J. A. Montgomery, J. Comput. Chem. **14**, 1347 (1993).
[55]G. Karlström, R. Lindh, P.-Å. Malmqvist, B. O. Roos, U. Ryde, V. Veryazov, P. O. Widmark, M. Cossi, B. Schimmelpfennig, P. Neograd, and L. Seijo, Comput. Mater. Sci. **28**, 222 (2003).
[56]H.-J. Werner, P. J. Knowles, G. Knizia, F. R. Manby, and M. Schütz, Comput. Mol. Sci. **2**, 242 (2012), available at http://onlinelibrary.wiley.com/doi/10.1002/wcms.82/pdf.
[57]H.-J. Werner, P. J. Knowles, F. R. Manby, M. Schütz *et al.*, MOLPRO, version 2010.1, a package of *ab initio* programs, 2010, see http://www.molpro.net.
[58]H. A. Witek, Y.-K. Choe, J. P. Finley, and K. Hirao, J. Comput. Chem. **23**, 957 (2002).
[59]T. H. Dunning, Jr., J. Chem. Phys. **90**, 1007 (1989).
[60]R. A. Kendall, T. H. Dunning, Jr., and R. J. Harrison, J. Chem. Phys. **96**, 6796 (1992).
[61]J. Oddershede, N. E. Grüner, and G. H. F. Diercksen, Chem. Phys. **97**, 303 (1985).
[62]See supplementary material at http://dx.doi.org/10.1063/1.4757264 for the computational details used in the test calculations.
[63]A. J. C. Varandas, J. Chem. Phys. **131**, 124128 (2009).
[64]B. O. Roos, R. Lindh, P.-Å. Malmqvist, V. Veryazov, and P.-O. Widmark, J. Phys. Chem. A **109**, 6575 (2005).
[65]M. F. Rode and H.-J. Werner, Theor. Chem. Acc. **114**, 309 (2005).
[66]K. R. Shamasundar, G. Knizia, and H.-J. Werner, J. Chem. Phys. **135**, 054101 (2011).
[67]M. Flock and K. Pierloot, J. Phys. Chem. A **103**, 95 (1999).
[68]C. J. Cramer, M. Włoch, P. Piecuch, C. Puzzarini, and L. Gagliardi, J. Phys. Chem. A **110**, 1991 (2006).
[69]M. Dolg, U. Wedig, H. Stoll, and H. Preuss, J. Chem. Phys. **86**, 866 (1987).
[70]T. H. Dunning, Jr., J. Chem. Phys. **53**, 2823 (1970).
[71]H. Han, B. Suo, D. Xie, Y. Wang, and Z. Wen, Phys. Chem. Chem. Phys. **13**, 2723 (2011)
[72]H. Han, B. Suo, Z. Jiang, Y. Wang, and Z. Wen, J. Chem. Phys. **128**, 184312 (2008).
[73]Q. Peng, Y. Wang, B. Suo, Q. Shi, and Z. Wen, J. Chem. Phys. **121**, 778 (2004).
[74]A. Li, Y. Dou, and Z. Wen, Chem. Phys. Lett. **478**, 28 (2009).
[75]Y. Lei, B. Suo, A. Li, Y. Dou, Y. Wang, and Z. Wen, Int. J. Quan. Chem **108**, 788 (2008).